

Search for the process $e^+e^- \rightarrow \eta'\gamma$ in the energy range $\sqrt{s} = 1.075 - 2$ GeV

M. N. Achasov,^{1,2} A. Yu. Barnyakov,^{1,2,3} E. V. Bedarev,^{1,2} K. I. Beloborodov,^{1,2} A. V. Berdyugin,^{1,2,*}
A. G. Bogdanchikov,¹ A. A. Botov,¹ T. V. Dimova,^{1,2} V. P. Druzhinin,^{1,2} V. N. Zhabin,^{1,2}
Yu.M.Zharinov,¹ L. V. Kardapoltsev,^{1,2} A. S. Kasaev,¹ A. A. Kattsin,¹ A. N. Kyrpotin,¹
D. P. Kovrizhin,¹ I. A. Koop,^{1,2} A. A. Korol,^{1,2} A. S. Kupich,^{1,2} A. P. Kryukov,¹ N. A. Melnikova,^{1,2}
N. Yu. Muchnoy,^{1,2} A. E. Obrazovskiy,¹ E. V. Pakhtusova,¹ K. V. Pugachev,^{1,2} S. A. Rastigeev,¹
Yu. A. Rogovsky,^{1,2} A. I. Senchenko,¹ S. I. Serebnyakov,^{1,2} Z. K. Silagadze,^{1,2} I. K. Surin,¹ Yu. V. Usov,¹
A. G. Kharlamov,^{1,2} D.E.Chistyakov,^{1,2} Yu. M. Shatunov,^{1,2} S. P. Sherstyuk,^{1,2} and D. A. Shtol¹

(SND Collaboration)

¹*Budker Institute of Nuclear Physics, SB RAS, Novosibirsk, 630090, Russia*

²*Novosibirsk State University, Novosibirsk, 630090, Russia*

³*Novosibirsk State Technical University, Novosibirsk, 630073, Russia*

The results of the search for the $e^+e^- \rightarrow \eta'\gamma$ process in the center-of-mass energy range from 1.075 to 2 GeV are presented. We analyze data with an integral luminosity of 746 pb⁻¹ accumulated with the SND detector at the e^+e^- collider VEPP-2000 in 2010–2024. The $\eta' \rightarrow \eta\pi^0\pi^0$ decay is used in the analysis, with the subsequent η and π^0 decays into $\gamma\gamma$. Upper limits not exceeding 13 pb have been set on the $e^+e^- \rightarrow \eta'\gamma$ cross section at the 90% confidence level.

I. INTRODUCTION

This work is devoted to the measurement of the $e^+e^- \rightarrow \eta'\gamma$ cross section with the SND detector at the VEPP-2000 collider [1] in the center-of-mass energy region $1.075 < \sqrt{s} < 2$ GeV. The process $e^+e^- \rightarrow \eta'\gamma$ is poorly studied experimentally. The vector mesons decays ϕ , J/ψ , and $\psi(2S)$ to $\eta'\gamma$ [2] and the cross section at $\sqrt{s} = 3.773$ GeV [3] and 10.6 GeV [4] were measured. In the energy region under study, there are the SND results [5] obtained using 12% of the SND data collected to date. In the work [5] the upper limits on the cross-section are set at the 90% confidence level (CL): $\sigma_{\eta'\gamma} < 28$ pb at $1.15 < \sqrt{s} < 1.39$ GeV and $\sigma_{\eta'\gamma} < 12$ pb at $1.39 < \sqrt{s} < 2.00$ GeV.

In the energy range from ϕ meson to 2 GeV, the e^+e^- annihilation into hadrons is dominated by contributions of excited vector resonances of the ρ , ω , and ϕ families. Therefore, we can expect that the $e^+e^- \rightarrow \eta'\gamma$ cross section will be determined by the radiative decays of these resonances. The quark model [6] predicts relatively large decay widths to $\eta'\gamma$ for the $\rho(1450)$ (60 keV) and $\phi(1680)$ (20 keV) states. Taking the $\rho(1450)$ and $\phi(1680)$ production cross section in e^+e^- annihilation of 60 nb and 13 nb, respectively, we can estimate the corresponding cross sections $\sigma(e^+e^- \rightarrow \rho(1450) \rightarrow \eta'\gamma) \approx 9$ pb and $\sigma(e^+e^- \rightarrow \phi(1680) \rightarrow \eta'\gamma) \approx 2$ pb.

In this work, we expect to reach the sensitivity of the $e^+e^- \rightarrow \eta'\gamma$ cross section measurement at the level of the quark model predictions.

II. DETECTOR AND EXPERIMENT

To search for the process $e^+e^- \rightarrow \eta'\gamma$, we use data with an integral luminosity of about 746 pb⁻¹ collected with the SND detector [7] at the VEPP-2000 e^+e^- collider from 2010 to 2024. The energy region 1.05–2.00 GeV was scanned several times with a step of 20–25 MeV. In this analysis, due to the small value of the cross section, a small set of statistics was obtained, and therefore we present as the result the cross section values averaged over 4 energy intervals listed in the table I.

A detailed description of the SND detector is given in Refs. [7]. This is a non-magnetic detector, the main part of which is a three-layer spherical electromagnetic calorimeter based on NaI(Tl) crystals. The solid angle of the calorimeter is 95% of 4π . Its energy resolution for photons is $\sigma_E/E = 4.2\%/ \sqrt{E(\text{GeV})}$, and its angular resolution is about 1.5°. The angles and production vertex of charged particles are measured in a tracking system consisting of a nine-layer drift chamber and a proportional chamber with cathode-strip readout. The track-system solid angle is 94% of 4π .

The search for the $e^+e^- \rightarrow \eta'\gamma$ process was discovered in the $\eta' \rightarrow \eta\pi^0\pi^0$ decay channel, with subsequent decays η - and π^0 -mesons in $\gamma\gamma$. Since the final state for the process under study does not contain charged particles, the process $e^+e^- \rightarrow \gamma\gamma$ is chosen for normalization. As a result of this normalization, the systematic uncertainties associated with the event selection in the first level trigger, as well as the uncertainties arising due to superimposing of beam-generated background charged tracks on events under study, are canceled. The accuracy of the luminosity measurement using the $e^+e^- \rightarrow \gamma\gamma$ process is 2.2% [8].

* A.V.Berdyugin@inp.nsk.su

III. EVENT SELECTION

The process under study

$$e^+e^- \rightarrow \eta'\gamma \rightarrow \eta\pi^0\pi^0\gamma \rightarrow 7\gamma \quad (1)$$

contains seven photons in the final state. Therefore, we select events with exactly seven reconstructed photons with energy greater 20 MeV and no charged tracks. The total energy deposition in the calorimeter E_{tot} and the total event momentum P_{tot} calculated using the energy depositions in the calorimeter crystals are required to satisfy the following conditions:

$$\begin{aligned} 0.7 < E_{\text{tot}}/\sqrt{s} < 1.2, \\ P_{\text{tot}}/\sqrt{s} < 0.3, \\ E_{\text{tot}}/\sqrt{s} - P_{\text{tot}}/\sqrt{s} > 0.7. \end{aligned} \quad (2)$$

For selected events, kinematic fits are performed using measured photon angles and energies, energy-momentum conservation laws, and assumptions about the presence of intermediate π^0 and η mesons. As a result of the fit, the photon energies are refined and χ^2 is calculated for the used kinematic hypothesis. Two hypotheses are tested:

- $e^+e^- \rightarrow 7\gamma$ ($\chi_{7\gamma}^2$),
- $e^+e^- \rightarrow \eta\pi^0\pi^0\gamma \rightarrow 7\gamma$ ($\chi_{\eta\pi^0\pi^0\gamma}^2$).

Events with $\chi_{\eta\pi^0\pi^0\gamma}^2 < 50$ are selected for further analysis.

The main sources of background are the processes $e^+e^- \rightarrow \omega\eta\pi^0$, $e^+e^- \rightarrow \omega\pi^0\pi^0$, $e^+e^- \rightarrow \eta\gamma$, $e^+e^- \rightarrow \pi^0\pi^0\gamma$, $e^+e^- \rightarrow \eta\pi^0\gamma$, and $e^+e^- \rightarrow \eta\eta\gamma$ with the decays $\omega \rightarrow \pi^0\gamma$, $\eta \rightarrow 3\pi^0$ or $\gamma\gamma$. Processes with neutral kaons in the final state $e^+e^- \rightarrow K_S K_L(\gamma)$, $e^+e^- \rightarrow K_S K_L \pi^0$, $e^+e^- \rightarrow K_S K_L \pi^0 \pi^0$, and $e^+e^- \rightarrow K_S K_L \eta$ with the decay $K_S \rightarrow 2\pi^0$ also contribute to the background. In processes with the K_L meson, additional photons originate from the K_L nuclear interaction in the calorimeter or its decay. Also, additional photons arise from splitting of electromagnetic showers, emission of photons by the initial particles at a large angle, and superimposing of beam-generated background.

Photon parameters obtained after the kinematic fit in the $e^+e^- \rightarrow 7\gamma$ hypothesis are used to suppress the background. The events containing three pairs of photons with an invariant mass satisfying the condition $|M_{\gamma\gamma} - M_{\pi^0}| < 35$ MeV were rejected. To suppress the background from processes containing the ω -meson, all possible three-photon combinations in an event are tested. If a combination with the three-photon invariant mass $|M_{3\gamma} - M_\omega| < 35$ MeV and the invariant mass of two of the three photons $|M_{\gamma\gamma} - M_{\pi^0}| < 35$ MeV is found, the event is rejected.

To determine the number of $\eta'\gamma$ events, we analyze the distribution over the invariant recoil mass against the photon M_{rec} , calculated after the kinematic fit in the hypothesis $e^+e^- \rightarrow \eta\pi^0\pi^0\gamma$. This distribution in the

range $850 < M_{\text{rec}} < 1250$ MeV for all selected events is shown in Fig. 1.

It is fitted by a sum of signal and background:

$$P(M_{\text{rec}}) = N_{\eta'\gamma} P_{\eta'\gamma}(M_{\text{rec}}) + N_{\text{bkg}} P_{\text{bkg}}(M_{\text{rec}}), \quad (3)$$

where the functions $P_{\eta'\gamma}$ and P_{bkg} are normalized to unity. The free fit parameters are the numbers of signal ($N_{\eta'\gamma}$) and background (N_{bkg}) events.

The signal line shape is obtained from simulation and then fitted by a sum of three Gaussian functions. The distribution for background is also determined from simulation. The contributions of various background processes are calculated using experimental data for the cross sections for $e^+e^- \rightarrow \eta\gamma$ [9], $e^+e^- \rightarrow \pi^0\pi^0\gamma$ [10], $e^+e^- \rightarrow \eta\pi^0\gamma$ [11, 12], $e^+e^- \rightarrow \eta\eta\gamma$ [11, 13], $e^+e^- \rightarrow \omega\pi^+\pi^-$ [14, 15], $e^+e^- \rightarrow \omega\eta\pi^0$ [16–18], $e^+e^- \rightarrow K_S K_L(\gamma)$ [19], $e^+e^- \rightarrow K_S K_L \pi^0$ [20, 21], $e^+e^- \rightarrow K_S K_L \pi^0 \pi^0$ [20], and $e^+e^- \rightarrow K_S K_L \eta$ [20]. For the process $e^+e^- \rightarrow \omega\pi^0\pi^0$, the isotopic relation $\sigma(\omega\pi^+\pi^-) = 2\sigma(\omega\pi^0\pi^0)$ is used. Upon calculation the background, radiation corrections [22] are taken into account. This is especially important for the processes $e^+e^- \rightarrow K_S K_L(\gamma)$ and $e^+e^- \rightarrow \eta\gamma(\gamma)$, which are dominated by “radiative return” to the ϕ meson, i.e. the processes $e^+e^- \rightarrow \phi\gamma \rightarrow K_S K_L \gamma$ and $e^+e^- \rightarrow \phi\gamma \rightarrow \eta\gamma\gamma$. In the energy region above 1.6 GeV, the cross sections of some background processes are known with poor accuracy ($\sim 25\%$). The expected distribution of the total background obtained from simulation (3) is normalized to unity and fitted by a sum of three Gaussian functions.

The result of the fit to the M_{rec} spectrum by Eq. (3) is shown in Fig. 1. It is seen that the simulation reproduces the shape of the background reasonably well. The number of background events 290 ± 20 found in the fit is consistent with that expected from simulation 230 ± 50 . The number of $e^+e^- \rightarrow \eta'\gamma$ events is equal to $N_{\eta'\gamma} = 25 \pm 8$. The significance of signal observation obtained from the difference between the likelihood functions of the fit described above and the fit with $N_{\eta'\gamma} = 0$ is found to be 4σ .

A similar fit is performed for the M_{rec} distributions in the four energy intervals. The obtained numbers of events of the signal and background are listed in Table I.

IV. DETECTION EFFICIENCY

The detection efficiency of the process under study is determined using Monte-Carlo simulation, which takes into account radiative corrections to the initial state, in particular, the emission of additional photons. The angular distribution of these photons is generated according to Ref. [23]. Fig. 2 shows the dependence of the detection efficiency $\varepsilon(\sqrt{s}, E_{\gamma_{\text{ISR}}})$ on the energy of the photon emitted from the initial state $E_{\gamma_{\text{ISR}}}$ at three center-of-mass energies.

The values of the detection efficiency at $E_{\gamma_{\text{ISR}}} = 0$ averaged over the energy intervals are listed in Table I.

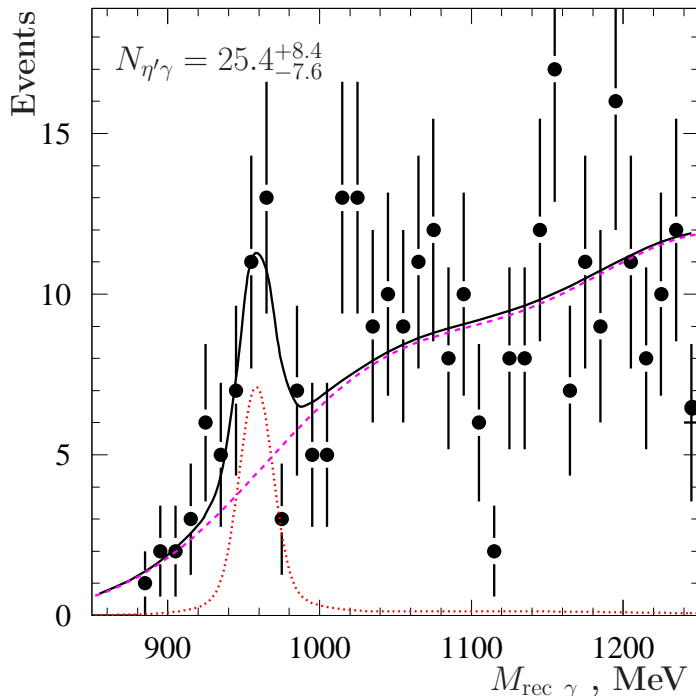


FIG. 1. The M_{rec} distribution for all selected data events (points with error bars). The solid curve represents the result of the fit described in the text. The dashed curve shows the fitted background contribution. The dotted curve is the signal line shape.

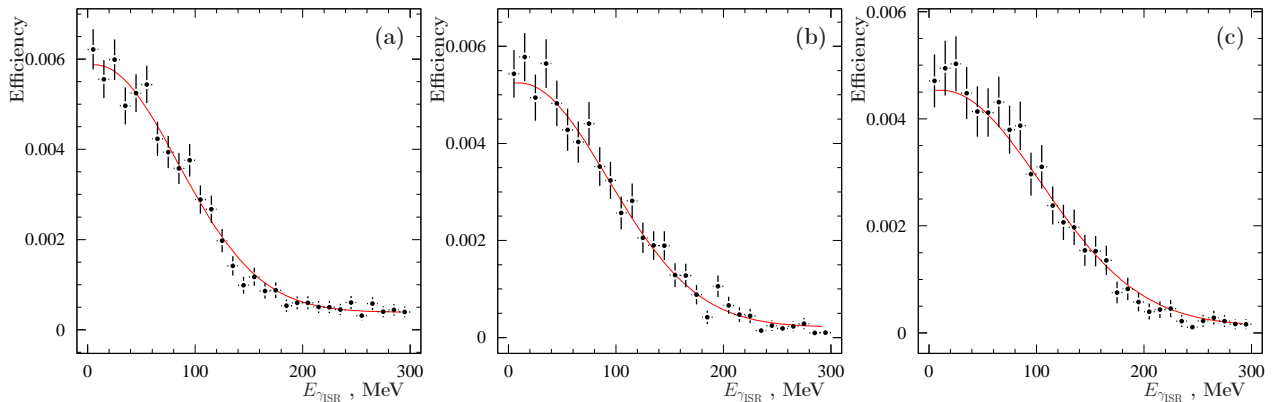


FIG. 2. The dependence of the detection efficiency for the $e^+e^- \rightarrow \eta'\gamma(\gamma)$ process on the energy of the additional photon emitted by the initial particles at $\sqrt{s} = 1.5$ GeV (a), 1.72 GeV (b), and 1.878 GeV (c). The points with error bars represent the simulation distribution. The curve is the result of the fit by a smooth function.

V. BORN CROSS SECTION

The visible cross section for the process $e^+e^- \rightarrow \eta'\gamma$ directly measured in experiment is related to the Born cross section ($\sigma(\sqrt{s})$) by the following formula:

$$\sigma_{\text{vis}}(\sqrt{s}) = \int_0^{x_{\text{max}}} \varepsilon\left(\sqrt{s}, \frac{x\sqrt{s}}{2}\right) F(x, \sqrt{s}) \sigma(\sqrt{s(1-x)}) dx, \quad (4)$$

where $F(x, \sqrt{s})$ is a function describing the distribution over the energy fraction $x = 2E_{\gamma\text{ISR}}/\sqrt{s}$ carried away by photons emitted from the initial state [22], $x_{\text{max}} = 1 - m_{\eta'}^2/s$. The expression (4) can be rewritten as:

$$\sigma_{\text{vis}}(\sqrt{s}) = \varepsilon_0(\sqrt{s}) \sigma(\sqrt{s}) (1 + \delta(\sqrt{s})), \quad (5)$$

where the detection efficiency $\varepsilon_0(\sqrt{s})$ and the radiative correction $\delta(\sqrt{s})$ are defined as follows:

$$\varepsilon_0(\sqrt{s}) \equiv \varepsilon(\sqrt{s}, 0), \quad (6)$$

$$\delta(\sqrt{s}) = \frac{\int_0^{x_{\max}} \varepsilon\left(\sqrt{s}, \frac{x\sqrt{s}}{2}\right) F(x, \sqrt{s}) \sigma\left(\sqrt{(1-x)s}\right) dx}{\varepsilon(\sqrt{s}, 0)\sigma(\sqrt{s})} - 1. \quad (7)$$

Technically, the Born cross section is determined as follows. The energy dependence of the measured visible cross section $\sigma_{\text{vis}}(\sqrt{s_i}) = N_{\eta'\gamma, i}/IL_i$, where i is the energy interval number, is fitted with Eq. (4). To parameterize the Born cross section, a theoretical model that describes the data well was chosen. With the obtained parameters of the theoretical model, the radiation correction $\delta(\sqrt{s_i})$ is determined by Eq. (7), and then the experimental Born cross section $\sigma(\sqrt{s_i})$ is calculated by Eq. (5).

To approximate the cross section, a model with one effective resonance is used:

$$\sigma_{\eta'\gamma}(\sqrt{s}) = \left(\frac{k_\gamma(\sqrt{s})}{\sqrt{s}}\right)^3 \cdot \left| \frac{m_V \Gamma_V(m_V)}{m_V^2 - s - i\sqrt{s}\Gamma_V} \sqrt{\frac{m_V^3}{k_\gamma(m_V)^3} \sigma_{V\eta'\gamma}} \right|^2, \quad (8)$$

$$k_\gamma(\sqrt{s}) = \frac{\sqrt{s}}{2} \left(1 - \frac{m_{\eta'}^2}{s}\right), \quad (9)$$

where m_V and $\Gamma_V(\sqrt{s})$ are the resonance mass and total width, $\sigma_{V\eta'\gamma}$ is the cross section at the resonance maximum. The free fit parameters are m_V , Γ_V and $\sigma_{V\eta'\gamma}$. The radiative corrections calculated in this model are listed in Table I. The Born cross section values obtained using Eq. (5) are listed in Table I and shown in Fig. 3. The fitting curve is shown in Fig. 3 by a solid line.

To determine the model uncertainty of the radiation correction, the fits are performed with $V = \phi(1680)$ and $\phi(2170)$. The masses and widths of the resonances in this

case are fixed at Particle Data Group values [2]. The fit results are shown in Fig. 3. It is seen that all three models do not contradict the data. The difference between the radiative corrections calculated in the three models is used to estimate the model uncertainty listed in Table I.

In Table I, the statistical and systematic uncertainties for the cross section are quoted. The latter includes uncertainties of the detection efficiency (3.3%), luminosity measurements (2.2%), and radiation correction. A detailed study of the systematic uncertainties associated with the selection of multiphoton events was carried out in Refs. [8–10, 24]. This uncertainty is estimated to be 3%. Additionally it is necessary to add the uncertainty appearing due to the difference between data and simulation in the probability of photon conversion before the tracking system equal to 1.3%.

The obtained cross-section values in the first three energy intervals do not contradict zero. The significance of signal observation in the last interval is 2σ . Therefore, the last column of Table I also contains the upper limits on the cross section at the 90% CL.

VI. SUMMARY

This paper presents the results of the search for the $e^+e^- \rightarrow \eta'\gamma$ process in the center-of-mass energy range from 1.07 to 2.00 GeV. Data with an integrated luminosity of 746 pb^{-1} accumulated by the SND detector at the VEPP-2000 e^+e^- collider in 2010–2024 have been analyzed. The decay mode $\eta' \rightarrow \eta\pi^0\pi^0$ with the subsequent decays η and $\pi^0 \rightarrow \gamma\gamma$ has been used.

The significance of the $e^+e^- \rightarrow \eta'\gamma$ signal in the full selected data sample has been found to be 4σ . However, after dividing the data into 4 energy intervals, there is no interval with a significance greater than 2σ . The upper limit on the cross section has been determined as not exceeding 13 pb at the 90% CL. In the region of the $\rho(1450)$ resonance, the upper limit is 7.5 pb and is at the level of the quark model prediction [6].

-
- [1] D. Shwartz *et al.*, JACoW **IPAC2021**, TUPAB002 (2021).
[2] R. L. Workman *et al.*, (Particle Data Group), Prog. Theor. Exp. Phys. **2022**, 083C01 (2022).
[3] T. K. Pedlar *et al.* (CLEO Collaboration), Phys. Rev. D **79**, 111101 (2009).
[4] B. Aubert *et al.* (BABAR Collaboration), Phys. Rev. D **74**, 012002 (2006).
[5] M. N. Achasov *et al.*, (SND Collaboration), Phys. Atom. Nucl. **83**, 714 (2020).
[6] F. E. Close, A. Donnachie and Y. S. Kalashnikova, Phys. Rev. D **65**, 092003 (2002).
[7] M. N. Achasov *et al.*, Nucl. Instrum. Methods **598**, 31 (2009); V. M. Aulchenko *et al.*, Nucl. Instrum. Methods **598**, 102 (2009); A. Yu. Barnyakov *et al.*, Nucl. Instrum. Methods **598**, 163 (2009); V. M. Aulchenko *et al.*, Nucl. Instrum. Methods **598**, 340 (2009).
[8] M. N. Achasov *et al.*, (SND Collaboration), Phys. Rev. D **88**, 054013 (2013).
[9] M. N. Achasov *et al.*, (SND Collaboration), Phys. Rev. D **74**, 014016 (2006); Phys. Rev. D **76**, 077101 (2007).
[10] M. N. Achasov *et al.*, (SND Collaboration), Phys. Rev. D **94**, 112001 (2016).
[11] M. N. Achasov *et al.*, (SND Collaboration), Phys. Rev. D **99**, 112004 (2019).
[12] M. N. Achasov *et al.*, (SND Collaboration), Eur. Phys. J. C **80**, 1008 (2020).
[13] V. L. Ivanov *et al.*, (CMD-3 Collaboration), arXiv:1906.08006 [hep-ex].
[14] R. R. Akhmetshin *et al.*, (CMD-2 Collaboration), Phys. Lett. B **489**, 125 (2000).

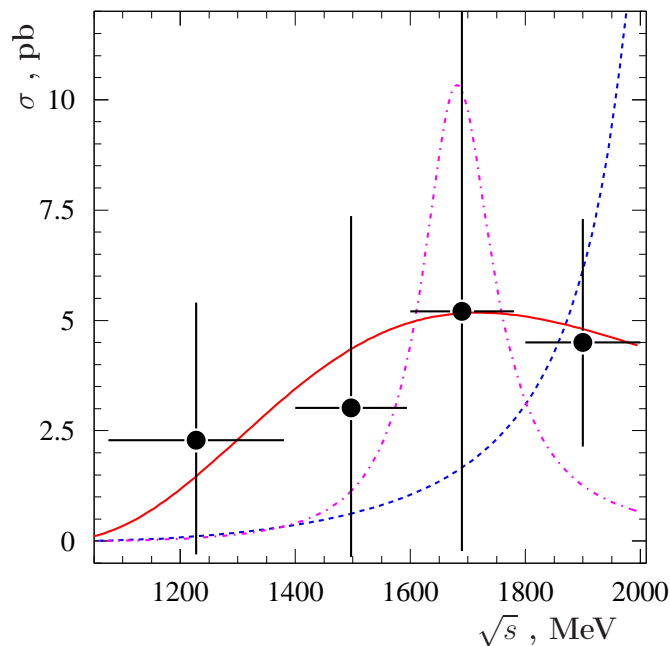


FIG. 3. The cross section for the process $e^+e^- \rightarrow \eta'\gamma$ measured in this work (points with error bars). The solid curve is the result of the fit with a resonance with free mass and width, the dashed and dash-dotted curves are the results of the fits with $\phi(2170)$ and $\phi(1680)$, respectively.

TABLE I. Energy interval (\sqrt{s}), integrated luminosity (IL), number of selected $e^+e^- \rightarrow \eta'\gamma$ events ($N_{\eta'\gamma}$), number of background events in the range $850 < M_{\text{rec}} < 1250$ MeV (N_{bkg}), obtained from the fit to M_{rec} spectrum and calculated using simulation, detection efficiency (ϵ_0), radiation correction ($1 + \delta$), and Born cross section for the process $e^+e^- \rightarrow \eta'\gamma$ ($\sigma_{\eta'\gamma}$). The first error in the cross section is statistical, the second is systematic. The upper limit on the cross section at the 90% CL is given in parentheses.

\sqrt{s} , GeV	IL , pb^{-1}	$N_{\eta'\gamma}$	N_{bkg}	ϵ_0 , %	$1 + \delta$	$\sigma_{\eta'\gamma}$, pb
1.075–1.38	201	$3.8^{+5.2}_{-4.3}$	$69 \pm 9 / 48 \pm 5$	0.89	0.87 ± 0.01	$2.3^{+3.1}_{-2.6} \pm 0.1$ (< 5.8)
1.4–1.594	120	$2.5^{+3.6}_{-2.8}$	$45 \pm 7 / 26 \pm 6$	0.74	0.90 ± 0.06	$2.9^{+4.1}_{-3.2} \pm 0.2$ (< 7.5)
1.6–1.78	99	$2.4^{+3.3}_{-2.5}$	$39 \pm 7 / 32 \pm 8$	0.60	0.90 ± 0.01	$5.1^{+7.0}_{-5.3} \pm 0.2$ (< 13.1)
1.8–2.0	326	$8.2^{+5.1}_{-4.3}$	$139 \pm 12 / 121 \pm 21$	0.54	0.91 ± 0.16	$5.0^{+3.1}_{-2.7} \pm 1.0$ (< 8.6)

- [15] B. Aubert *et al.*, (BABAR Collaboration), Phys. Rev. D **76**, 092005 (2007); Phys. Rev. D **77**, 119902 (Erratum) (2008).
- [16] M. N. Achasov *et al.*, (SND Collaboration), Phys. Rev. D **94**, 032010 (2016).
- [17] J. P. Lees *et al.*, (BABAR Collaboration), Phys. Rev. D **98**, 112015 (2018).
- [18] J. P. Lees *et al.*, (BABAR Collaboration), Phys. Rev. D **103**, 092001 (2021).
- [19] J. P. Lees *et al.*, (BABAR Collaboration) Phys. Rev. D **89**, 092002 (2014).
- [20] J. P. Lees *et al.*, (BABAR Collaboration), Phys. Rev. D **95**, 052001 (2017).
- [21] M. N. Achasov *et al.*, (SND Collaboration), Phys. Rev. D **97**, 032011 (2018).
- [22] E. A. Kuraev and V. S. Fadin, Yad. Fiz. **41**, 733 (1985) [Sov. J. Nucl. Phys. **41**, 466 (1985)].
- [23] G. Bonneau and F. Martin, Nucl. Phys. B **27**, 381 (1971).
- [24] M. N. Achasov *et al.*, (SND Collaboration), Phys. Rev. D **90**, 032002 (2014).